Phase-sensitive cascaded four-wave-mixing processes for generating three quantum correlated beams

Li Wang,[1] Hailong Wang,[1] Sijin Li,[1] Yaxian Wang,[1] and Jietai Jing[1,2,*]

[1]*State Key Laboratory of Precision Spectroscopy, School of Physics and Materials Science, East China Normal University, Shanghai 200062, China*

[2]*Collaborative Innovation Center of Extreme Optics, Shanxi University, Taiyuan, Shanxi 030006, China*

(Received 20 April 2016; revised manuscript received 25 August 2016; published 5 January 2017)

Theoretical studies and experimental implementations of quantum correlation are the important contents of continuous variables quantum optics and quantum information science. There are various systems for the study of quantum correlation. Here, we study an experimental scheme for generating three quantum correlated beams based on phase-sensitive cascaded four-wave-mixing (FWM) processes in rubidium vapor. Quantum correlation including intensity difference or sum squeezing, two other combinatorial squeezing, and quantum entanglement among the three output light fields are theoretically analyzed in this paper. Also, the comparison of the quantum correlations have been made between the phase-sensitive cascaded FWM processes and the phase-insensitive cascaded FWM processes. By changing the phases and intensities of the input beams, it is interesting to find that the maximum degrees of various combinatorial squeezing are equal when the two FWM processes share a common intensity gain. When the common intensity gain of the two FWM processes changes, the maximum degrees of different combinatorial squeezing will be synchronously controlled. At last we discuss the genuine tripartite entanglement and steering in our phase-sensitive cascaded scheme, and compare them with the cases of the phase-insensitive cascaded scheme.

DOI: 10.1103/PhysRevA.95.013811

I. INTRODUCTION

Multimode quantum states, which are quantum correlations shared and distributed among multiple parties, have attracted considerable attention because of their fundamental scientific significance [1,2] and potential applications in future quantum technologies [3,4]. A number of different techniques for its generation have been proposed and experimentally implemented. For example, one approach pursued in this area is to use independent single mode squeezed beams generated by optical parametric oscillators (OPOs), together with multiple beamsplitters to generate a continuous variable (CV) quantum network [5]. Such linear beamsplitter network has been experimentally realized by several groups [6–8]. Other groups have experimentally followed another promising approach with a single multimode nonlinear process using different spatial regions of a single beam [9], multiple longitudinal [10], or temporal modes [11]. Recent advances in this respect include the ultralarge-scale quantum networks generated in both the time [12] and the frequency domains [13,14].

In 2007, Paul Lett's group at NIST experimentally generated a pair of intensity-correlated beams based on the nondegenerate four-wave-mixing (FWM) process in a hot rubidium vapor [15]. This system has several advantages for practical implementations, e.g., no need of a cavity due to the strong nonlinearity of the system, a spatial multimode nature due to no mode constraint, spatial separation of the generated nonclassical beams, etc. These advantages explain the rapidly growing popularity of such a system in many applications, including quantum information processing and quantum metrology, such as entangled images [16], tunable delay of EPR entanglement [17], nonlinear quantum interferometer [18–20], high purity narrow-bandwidth single photons [21], ultrasensitive measurement of microcantilever displacement [22], and the localized multispatial mode quadrature squeezing for quantum imaging [23].

Due to these advantages, it is a good candidate for generating multiple quantum correlated beams which have potential applications in quantum communication [3,4,24–28]. For example, theoretical proposals based on FWM in hot vapor have been proposed to realize CV cluster state generation over a spatial comb through the FWM process [29] and versatile quantum network generation by cascading several FWM processes [30]. In 2014, our group has experimentally generated three bright strongly quantum correlated beams by phase-insensitive cascaded FWM processes in hot vapors [19].

The gain and noise of the phase-insensitive amplification process are independent of the phases of the input signals. The output of such a process necessarily has a lower signal-to-noise ratio (SNR) than the input. In contrast, the gain and noise of the phase-sensitive amplification process are dependent of the phases of the input signal. The phase-sensitive amplification process will not degrade the SNR with a correct choice of the phases of the input signals. For this reason, in this paper, we mainly study an experimental scheme for generating three quantum correlated beams based on phase-sensitive cascaded FWM processes in Rb vapor. Compared with the linear beamsplitter network [5–8] that passively mixes squeezed states, our cascaded FWM processes based scheme actively constructs and even enhances quantum correlation among the output modes. Quantum correlation including intensity difference or sum squeezing, two other combinatorial squeezing, and genuine tripartite entanglement and steering among the three output light fields are theoretically analyzed. Compared with the degree of intensity difference squeezing of the twin output beams obtained with phase-sensitive single FWM process [31] or the three output beams obtained with phase-insensitive

*Corresponding author: jtjing@phy.ecnu.edu.cn

cascaded FWM processes [32], the degree of intensity difference squeezing of the three beams output from the current phase-sensitive cascaded FWM processes can be largely enhanced. No matter what kind of combination, it is worth noting that the maximal squeezing levels would always be equal when the two FWM processes share a common intensity gain. When the common intensity gain of the two FWM processes changes, the maximum degree of different combinatorial squeezing will be synchronously controlled. Then we discuss the tripartite entanglement in our phase-sensitive cascaded FWM processes by using the single-condition criterion and the two-condition criterion [33], and compare them with the cases of the phase-insensitive cascaded FWM processes. Further, we investigate the multipartite steering [34,35] based on our cascaded FWM processes. We find that there exists genuine tripartite steering in our cascaded scheme. Additionally, not only the light intensity of the output probe beam but also the signal-to-noise ratio (SNR) of it can be improved by changing the phases and intensities of the input beams.

This paper is organized as follows. In the second section, phase-sensitive cascaded FWM processes are briefly introduced. The amplification and deamplification of the input probe field is briefly described in Sec. III. In Sec. IV, the noise properties of the system are also discussed. The ratio of the variance of the output probe field to the variance at the standard quantum limit (SQL) and the noise figure (NF) of the system are included in Sec. IV. Various combinatorial squeezing among the triple beams output from the current cascaded phase-sensitive FWM processes is deduced and the influences of the phases and the intensity ratios of the input beams are also theoretically analyzed in this section. The genuine tripartite entanglement and steering in cascaded FWM processes is discussed in Sec. V. Finally, a brief conclusion is given in Sec. VI.

II. PHASE-SENSITIVE CASCADED FWM PROCESSES

We use a double-λ FWM process in Rb atomic vapor as shown in Fig. 1(b). As shown in Fig. 1(a), two coherent fields, the probe ($\hat{a}_0$) and conjugate ($\hat{b}_0$) beams, are simultaneously and symmetrically crossed with a strong pump beam ($\hat{c}_1$) in the first atomic vapor. Probe ($\hat{a}_1$) and conjugate ($\hat{b}_1$) beams are created via the FWM scheme in the first Rb vapor. Then the probe beam ($\hat{a}_1$) is fed into a second FWM process with an additional phase θ_x caused by the distance between the two FWM processes. The probe beam ($\hat{a}_1 e^{i\theta_x}$) and the coherent conjugate beam ($\hat{b}'_0$) are also simultaneously and symmetrically crossed with a strong pump beam ($\hat{c}_2$) in the second Rb vapor. Then the probe ($\hat{a}_2$) and conjugate ($\hat{b}_2$) beams are created after the second Rb vapor. Viewing the two FWM processes as a whole system, there are three output light beams, which are the probe $\hat{a}_2$ ($\hat{O}_1$), conjugate $\hat{b}_2$ ($\hat{O}_2$), and another conjugate $\hat{b}_1$ ($\hat{O}_3$).

The FWM process involves the annihilation of two pump photons, and the creation of a single probe and a conjugate photon. Labeling the annihilation operator of the probe ($\hat{a}$), conjugate ($\hat{b}$), and pump ($\hat{c}$) respectively, the Hamiltonian ($\hat{H}_1$) and ($\hat{H}_2$) corresponding to the interaction of the first and the second FWM processes can be written by [36,37]

$$\hat{H}_1 = i\hbar\zeta_1 e^{-i\theta_1}\hat{b}^\dagger\hat{a}^\dagger + \text{H.c.}, \tag{1}$$

$$\hat{H}_2 = i\hbar\zeta_2 e^{-i\theta_2}\hat{b}^\dagger\hat{a}^\dagger + \text{H.c.}, \tag{2}$$

where the ζ_1 and ζ_2 are the interaction strength of the first and second FWM processes respectively that depend on the length of the interaction and are proportional to the intensities of pump light beams ($\hat{c}_1$) and ($\hat{c}_2$) respectively. The phases of the pump fields ($\hat{c}_1$) and ($\hat{c}_2$) can be shown as ϕ_{c_1} and ϕ_{c_2} respectively. Here θ_1 is equal to $2\phi_{c_1}$ and θ_2 is equal to $2\phi_{c_2}$. From Eq. (1), the time evolution of the first FWM process is given by

$$\hat{a}_1(t) = \sqrt{G_1}\hat{a}_0 + e^{i\theta_1}\sqrt{G_1 - 1}\hat{b}_0^\dagger, \tag{3}$$

$$\hat{b}_1^\dagger(t) = \sqrt{G_1}\hat{b}_0^\dagger + e^{-i\theta_1}\sqrt{G_1 - 1}\hat{a}_0. \tag{4}$$

From Eq. (2), the time evolution of the FWM process is given by

$$\hat{a}_2(t) = \sqrt{G_2}\hat{a}_1 e^{i\theta_x} + e^{i\theta_2}\sqrt{G_2 - 1}\hat{b}_0'^\dagger, \tag{5}$$

$$\hat{b}_2^\dagger(t) = \sqrt{G_2}\hat{b}_0'^\dagger + e^{-i\theta_2}\sqrt{G_2 - 1}\hat{a}_1 e^{i\theta_x}, \tag{6}$$

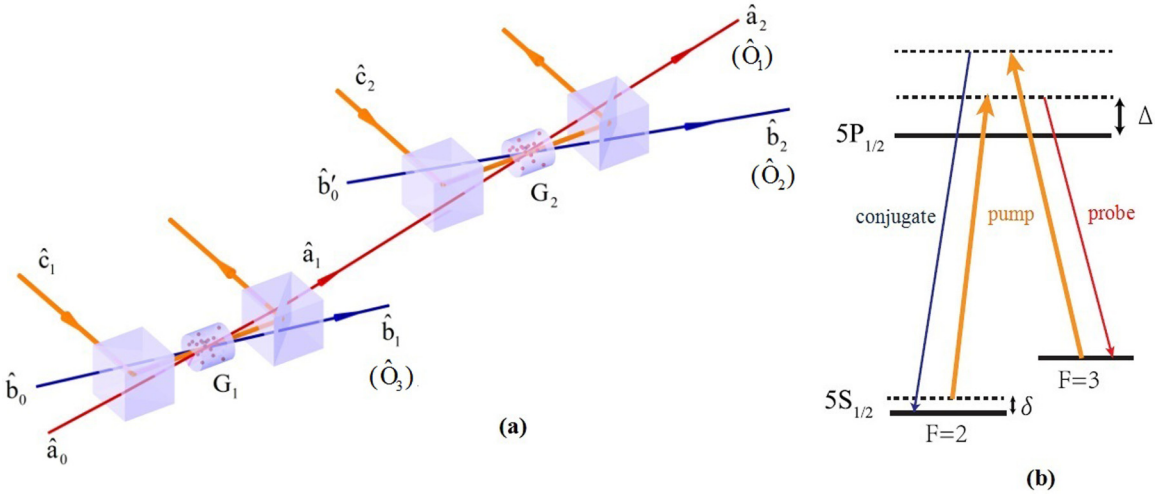

FIG. 1. Phase-sensitive cascaded FWM processes in hot ^{85}Rb vapor. (a) The experimental arrangement. (b) Double-λ energy level of ^{85}Rb $D1$ line: Δ and δ stand for the one-photon detuning and the two-photon detuning respectively. The interaction strength depends strongly on the one-photon detuning Δ and the two-photon detuning δ.

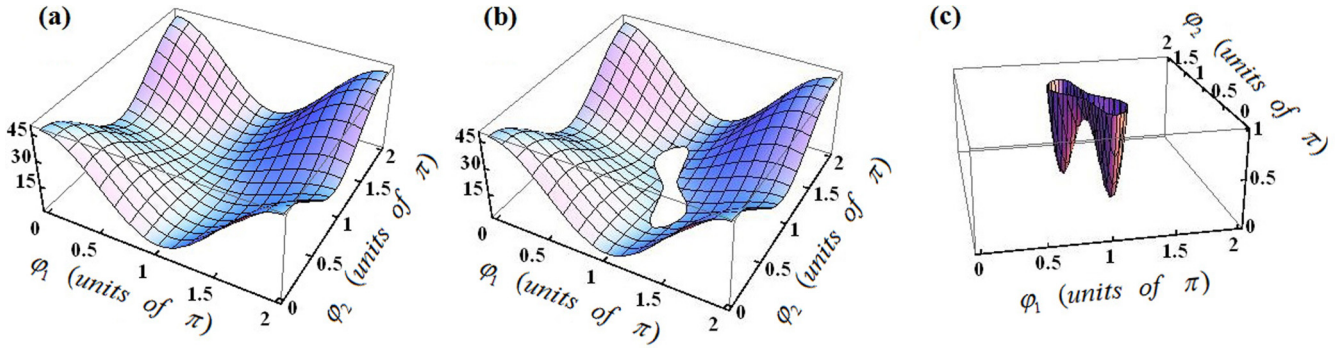

FIG. 2. The relation among $G_{\text{eff,probe}}$, φ_1 and φ_2 under the $\beta_1 = \beta_2 = 1$ condition. (a) The entire picture for $G_{\text{eff,probe}}$. (b) The local picture for $G_{\text{eff,probe}} > 1$. (c) The local picture for $G_{\text{eff,probe}} < 1$. Panel (b) shows the probe beam amplified. In addition, panel (c) shows the probe beam deamplified.

where θ_x represents the additional phase of the probe beam ($\hat{a}_1$) depending on the distance between the two FWM processes. Here $G_1 = \cosh\zeta_1 t$ and $G_2 = \cosh\zeta_2 t$ depend on the strength of the interaction. G_1 and G_2 are the intensity gain of the first and second FWM processes respectively. Through the use of Eqs. (3)–(6), the input-output relation of the whole system can be shown as Eq. (7):

$$\begin{pmatrix} \hat{a}_2(t) \\ \hat{b}_2^\dagger(t) \\ \hat{b}_1^\dagger(t) \end{pmatrix} = \begin{pmatrix} \sqrt{G_1 G_2}e^{i\theta_x} & \sqrt{(G_1-1)G_2}e^{i\theta_1+i\theta_x} & \sqrt{G_2-1}e^{i\theta_2} \\ \sqrt{G_1(G_2-1)}e^{i\theta_x-i\theta_2} & \sqrt{(G_1-1)(G_2-1)}e^{i\theta_1+i\theta_x-i\theta_2} & \sqrt{G_2} \\ \sqrt{G_1-1}e^{-i\theta_1} & \sqrt{G_1} & 0 \end{pmatrix} \begin{pmatrix} \hat{a}_0 \\ \hat{b}_0^\dagger \\ \hat{b}_0'^\dagger \end{pmatrix}. \tag{7}$$

III. AMPLIFICATION AND DE-AMPLIFICATION OF THE SYSTEM

The mean value of photon number operator ($\langle \hat{N}_{a_2,\text{out}} \rangle$) for the output probe mode ($\hat{a}_2$) is $\langle \hat{N}_{a_2,\text{out}} \rangle = \langle \hat{a}_2^\dagger \hat{a}_2 \rangle$, which through use of Eqs. (3) and (5) becomes

$$\begin{aligned} \langle \hat{N}_{a_2,\text{out}} \rangle &= G_1 G_2 \langle \hat{N}_{a_0} \rangle + (G_1 - 1) G_2 \langle \hat{N}_{b_0} \rangle \\ &+ (G_2 - 1)\langle \hat{N}_{b_0'} \rangle + (G_1 G_2 - 1) \\ &+ 2\sqrt{G_1(G_1-1)}G_2\sqrt{\langle \hat{N}_{a_0} \rangle \langle \hat{N}_{b_0} \rangle}\cos\varphi_1 \\ &+ 2\sqrt{G_1 G_2 (G_2-1)}\sqrt{\langle \hat{N}_{a_0} \rangle \langle \hat{N}_{b_0'} \rangle}\cos\varphi_2 \\ &+ 2\sqrt{(G_1-1)G_2(G_2-1)}\sqrt{\langle \hat{N}_{b_0} \rangle \langle \hat{N}_{b_0'} \rangle} \\ &\times \cos(\varphi_1 - \varphi_2), \end{aligned} \tag{8}$$

where $\langle \hat{N}_{a_0} \rangle$ and $\langle \hat{N}_{b_0} \rangle$ represent the average input photon number of the probe and conjugate fields fed in the first Rb vapor cell respectively. $\langle \hat{N}_{b_0'} \rangle$ represents the average input photon number of the conjugate field injected in the second Rb vapor cell. The phases of the probe field ($\hat{a}_0$) and the conjugate field ($\hat{b}_0$) can be denoted as ϕ_a and ϕ_b respectively. $\phi_{b'}$ represents the phase of another conjugate field ($\hat{b}_0'$). φ_1 is equal to $\theta_1 - \phi_a - \phi_b$ and φ_2 is equal to $\theta_2 - \theta_x - \phi_a - \phi_{b'}$. The term $(G_1 G_2 - 1)$ in Eq. (8), which is due to the spontaneous emission during the FWM processes, can be ignored when the probe beam ($\hat{a}_0$) is bright. When the conjugate ports ($\hat{b}_0$) and ($\hat{b}_0'$) are seeded with vacuum, which means $\langle \hat{N}_{b_0} \rangle = 0$ and $\langle \hat{N}_{b_0'} \rangle = 0$, the average output photon number of the probe is thus given by $\langle \hat{N}_{a,\text{out}} \rangle = G_1 G_2 \langle \hat{N}_{a_0} \rangle$. This agrees well with the result of the PIA shown in Ref. [32]. When the second Rb vapor cell is absent, that is to say, $\langle \hat{N}_{b_0'} \rangle = 0$ and $G_2 = 1$, we can then calculate the average output photon number of the probe beam. Obviously, it conforms to the conclusion that Ref. [31] has drawn.

From Eq. (8) we can see that the intensity of output probe field depends not only on the phase φ_1 and φ_2 but also on the intensity of the three input fields $\hat{a}_0$, $\hat{b}_0$, and $\hat{b}_0'$. Then we define the intensity ratio $\langle \hat{N}_{b_0} \rangle / \langle \hat{N}_{a_0} \rangle$ as β_1 and $\langle \hat{N}_{b_0'} \rangle / \langle \hat{N}_{a_0} \rangle$ as β_2. We can simplify Eq. (8) when $\beta_1 = \beta_2 = 1$,

$$\begin{aligned} \langle \hat{N}_{a_2,\text{out}} \rangle &= 2\sqrt{G_1(G_1-1)}G_2\langle \hat{N}_{a_0} \rangle \cos\varphi_1 + (2G_1 G_2 - 1)\langle \hat{N}_{a_0} \rangle \\ &+ 2\sqrt{G_1 G_2 (G_2-1)}\langle \hat{N}_{a_0} \rangle \cos\varphi_2 \\ &+ 2\sqrt{(G_1-1)G_2(G_2-1)}\langle \hat{N}_{a_0} \rangle \cos(\varphi_1 - \varphi_2). \end{aligned} \tag{9}$$

Then we can consider the effective gain for probe light, $G_{\text{eff,probe}} = \langle \hat{N}_{a,\text{out}} \rangle / \langle \hat{N}_{a_0} \rangle$, to study the amplification ($G_{\text{eff,probe}} > 1$) and deamplification ($G_{\text{eff,probe}} < 1$) of the probe beam. The effective gain $G_{\text{eff,probe}}$ is given by

$$\begin{aligned} G_{\text{eff,probe}} &= 2\sqrt{G_1(G_1-1)}G_2\cos\varphi_1 \\ &+ (2G_1 G_2 - 1) + 2\sqrt{G_1 G_2 (G_2-1)}\cos\varphi_2 \\ &+ 2\sqrt{(G_1-1)G_2(G_2-1)}\cos(\varphi_1 - \varphi_2). \end{aligned} \tag{10}$$

We assume that the intensity gain of the first and second FWM processes is equal to 3, $G_1 = G_2 = 3$, which results in $G_{\text{eff,probe}}$ changing with φ_1 and φ_2 [Fig. 2(a)]. As the phase φ_1 and φ_2 vary, the effective gain $G_{\text{eff,probe}}$ can vary between $G_{\text{eff,probe}} > 1$ [Fig. 2(b)] and $G_{\text{eff,probe}} < 1$ [Fig. 2(c)]. As shown in Fig. 2(b) [local image of Fig. 2(a)], it means the amplification of the probe beam. Another case is shown in

Fig. 2(c) [partial enlargement of Fig. 2(a)], where the probe beam is deamplified.

If we consider the two FWM processes as a whole system, we can treat the amplification or deamplification of the probe beam as constructive and destructive interference of input light beams respectively [31]. The two effective gain valleys as show in Fig. 2(c) that describe relatively complete destructive interference can be obtained with two sets of (φ_1,φ_2) in the case of $G_1 = G_2 = 3$ and $\beta_1 = \beta_2 = 1$. In fact, the two effective gain valleys are not a minimum value of effective gain in the case of $G_1 = G_2 = 3$. When the intensity gain of the two FWM processes is fixed, the effective gain of the probe beam will change with four variables: φ_1, φ_2, β_1, and β_2. That is to say, we can always find a minimum value of the effective gain by changing values of φ_1, φ_2, β_1, and β_2. In the situation of $G_1 = G_2 = 3$, the minimum value of effective gain can be achieved when $\varphi_1 = \varphi_2 = \pi$, $\beta_1 = 0.54$, and $\beta_2 = 0.72$. From the point of interference phenomena, the most complete destructive interference in the case of $G_1 = G_2 = 3$ is available when it meets the requirements of $\varphi_1 = \varphi_2 = \pi$, $\beta_1 = 0.54$, and $\beta_2 = 0.72$. Of course, the probe beam is maximally deamplified here.

IV. NOISE PROPERTIES OF THE SYSTEM

As discussed above, the probe beam could be amplified or deamplified under different conditions. However, some noise will thereby be introduced after the amplification or deamplification process [38]. It is useful to characterize the noise level of the probe beam by the ratio of the variance of the output to the variance at the SQL. The variance of the output mode is $\mathrm{Var}(\hat{N}_{a,\mathrm{out}}) = \langle \hat{a}_2^\dagger \hat{a}_2 \hat{a}_2^\dagger \hat{a}_2 \rangle - \langle \hat{a}_2^\dagger \hat{a}_2 \rangle \langle \hat{a}_2^\dagger \hat{a}_2 \rangle$ and $\mathrm{Var}(\hat{N}_{a,\mathrm{out}})_{\mathrm{SQL}}$ is equal to the mean value of the output photon number. Through use of Eqs. (3) and (5), the noise level of probe beam becomes

$$\frac{\mathrm{Var}(\hat{N}_{a,\mathrm{out}})}{\mathrm{Var}(\hat{N}_{a,\mathrm{out}})_{\mathrm{SQL}}} = 2G_1G_2 - 1. \tag{11}$$

This equation shows that the noise on the probe beam can become arbitrarily large for large values of the intensity gain G_1 and G_2. It is interesting to find this kind of additive noise is independent of the phases or the intensities of the input beams. Therefore this kind of system always introduces excess noise to the input signal [39]. In addition, we will show the noise properties of this system by means of its NF [38,40]. The NF (represented below as Z) is defined as the square of the ratio of signal-to-noise ratios of the input and output fields [41]

$$Z = \frac{(S/N)^2_{a_0}}{(S/N)^2_{a_2}}, \tag{12}$$

where

$$(S/N)^2_{a_0} = \frac{\langle \hat{N}_{a_0} \rangle^2}{\langle \triangle \hat{N}^2_{a_0} \rangle} \tag{13}$$

and

$$(S/N)^2_{a_2} = \frac{\langle \hat{N}_{a_2} \rangle^2}{\langle \triangle \hat{N}^2_{a_2} \rangle}. \tag{14}$$

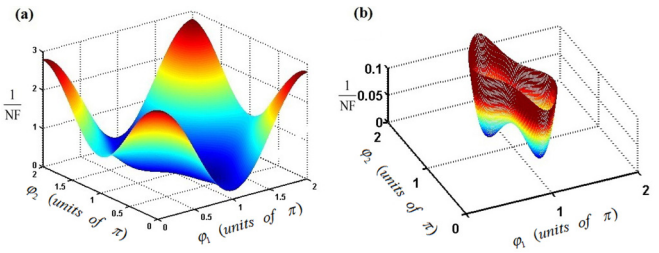

FIG. 3. $\frac{1}{Z}$ plotted as a function of the input phase φ_1 and φ_2. (a) The entire picture for $\frac{1}{Z}$ varies with phase φ_1 and φ_2. (b) The local picture for $\frac{1}{Z} < 0.1$.

It is interesting to examine how this NF varies with the phase φ_1 and φ_2. For convenience, we plot the inverse of NF, i.e., $\frac{1}{Z}$. In order to be consistent with earlier calculation, we set G_1, G_2 equal to 3 and β_1, β_2 equal to 1.

In Fig. 3, the $\frac{1}{Z}$ is plotted as a function of the phase φ_1 and φ_2 for the case in which $G_1 = G_2 = 3$ and $\beta_1 = \beta_2 = 1$. Because of constructive interference, the NF of this phase-sensitive process can be less than 1 ($\frac{1}{Z} > 1$), meaning that the SNR is enhanced by this whole process. The NF will become quite large ($\frac{1}{Z} < 1$) due to destructive interference, meaning that the SNR is getting worse. Furthermore, in Fig. 3(b), there are two valleys of $\frac{1}{Z}$, which correspond to the two relatively complete destructive interference.

Let us now consider the quantum variances of intensity difference or sum squeezing and other combinatorial squeezing among the three output light fields. The degree of squeezing [DS (represented below as D)] of the intensity difference among the three output light fields with respect to the SQL is given by

$$D_{\hat{N}_{a_2}-\hat{N}_{b_2}-\hat{N}_{b_1}} = 10\log_{10}\left(\frac{\mathrm{Var}\left(\hat{N}_{a_2} - \hat{N}_{b_2} - \hat{N}_{b_1}\right)}{\mathrm{Var}\left(\hat{N}_{a_2} - \hat{N}_{b_2} - \hat{N}_{b_1}\right)_{\mathrm{SQL}}}\right). \tag{15}$$

Here one can easily calculate the term $\mathrm{Var}(\hat{N}_{a_2} - \hat{N}_{b_2} - \hat{N}_{b_1})$ from Eq. (7), and $\mathrm{Var}(\hat{N}_{a_2} - \hat{N}_{b_2} - \hat{N}_{b_1})_{\mathrm{SQL}}$ is just the sum of the mean value of the output photon number. In order to be consistent with earlier calculation, we set the intensity gain to satisfy the relationship $G_1 = G_2 = 3$. Then the quantum variances of intensity difference squeezing among the three output light fields is simplified as

$$D_{\hat{N}_{a_2}-\hat{N}_{b_2}-\hat{N}_{b_1}} = 10\log_{10}\left(\frac{1+\beta_1+\beta_2}{\gamma}\right), \tag{16}$$

where γ is equal to $17 + 13\beta_1 + 5\beta_2 + 12\sqrt{6}\sqrt{\beta_1}\cos(\varphi_1) + 12\sqrt{2}\sqrt{\beta_2}\cos(\varphi_2) + 8\sqrt{3}\sqrt{\beta_1\beta_2}\cos(\varphi_1 - \varphi_2)$. When we seed vacuum fields to the conjugate ports $\hat{b}_0$ and $\hat{b}'_0$ ($\beta_1 = \beta_2 = 0$), the degree of intensity difference squeezing of the output beams is given by -12.3 dB ($10\log_{10}\frac{1}{17}$ dB), which agrees with the result $10\log_{10}(\frac{1}{2G^2-1})$ dB of a phase-insensitive cascaded scheme in Ref. [32]. Equation (16) shows that the degree of squeezing varies with the phase φ_1, φ_2 and the intensity ratio β_1, β_2. We can find the maximal squeezing by changing φ_1, φ_2, β_1, and β_2. In the current situation, the maximal squeezing is -15.311 dB which corresponds to $\beta_1 = 0.75$, $\beta_2 = 0.25$, and $\varphi_1 = \varphi_2 = 0, 2\pi$. Similarly, we can also find that the maximal squeezing levels of intensity

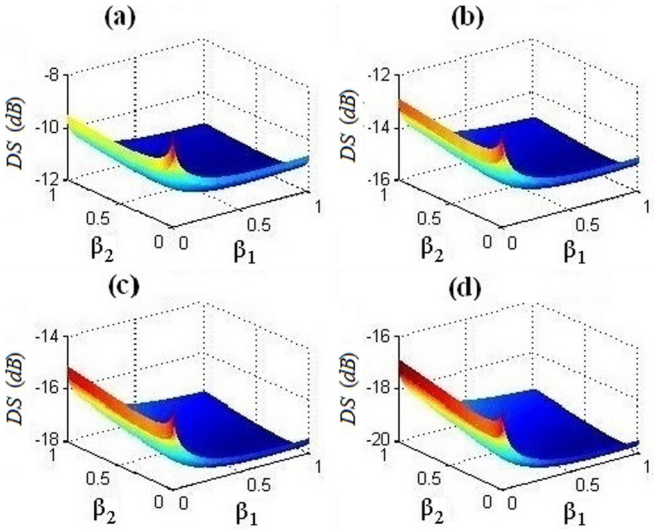

FIG. 4. The squeezing levels of intensity difference $D_{(\hat{N}_{a_2}-\hat{N}_{b_2}-\hat{N}_{b_1})}$ vary with β_1 and β_2 when $\varphi_1=\varphi_2=0/2\pi$. (a) $G_1=G_2=2$: The squeezing level becomes maximal when $\beta_1=0.667$ and $\beta_2=0.333$. (b) $G_1=G_2=3$: The squeezing level becomes maximal when $\beta_1=0.75$ and $\beta_2=0.25$. (c) $G_1=G_2=4$: The squeezing level becomes maximal when $\beta_1=0.8$ and $\beta_2=0.2$. (d) $G_1=G_2=5$: The squeezing level becomes maximal when $\beta_1=0.833$ and $\beta_2=0.167$.

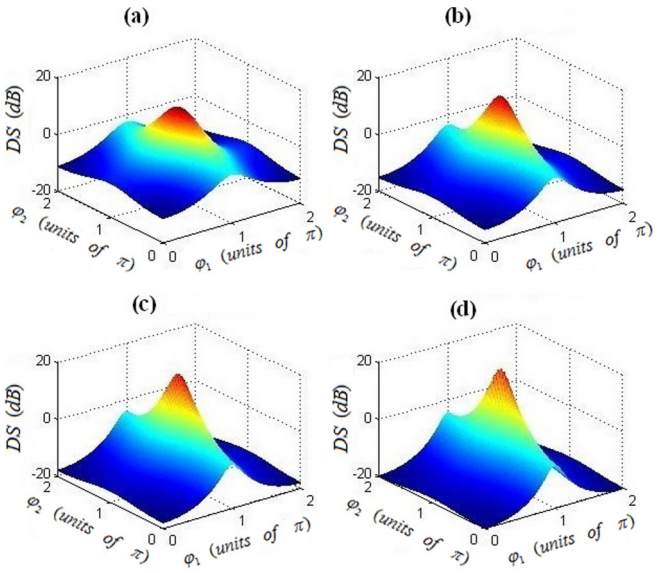

FIG. 5. (a) $G_1=G_2=2$: The squeezing level of intensity difference $D_{(\hat{N}_{a_2}-\hat{N}_{b_2}-\hat{N}_{b_1})}$ varies with the phase φ_1 and φ_2 when $\beta_1=0.667$ and $\beta_2=0.333$. (b) $G_1=G_2=3$: The squeezing level varies with the phases when $\beta_1=0.75$ and $\beta_2=0.25$. (c) $G_1=G_2=4$: The squeezing level varies with the phases when $\beta_1=0.8$ and $\beta_2=0.2$. (d) $G_1=G_2=5$: The squeezing level varies with the phases when $\beta_1=0.833$ and $\beta_2=0.167$. All of the squeezing levels for different gains become maximal when $\varphi_1=\varphi_2=0/2\pi$.

difference are -11.439, -17.923, and -19.913 dB which correspond to $G_1=G_2=2,4,5$ respectively. The maximal squeezing levels of intensity difference can be obtained when β_1,β_2 are certain values and $\varphi_1=\varphi_2=0,2\pi$. Then we plot the squeezing levels of intensity difference in decibels as a function of the ratio β_1, β_2 when $\varphi_1=\varphi_2=0,2\pi$ for intensity gains of 2, 3, 4, 5 as shown in Fig. 4. When $\varphi_1=\varphi_2=0,2\pi$, the maximal squeezing for different gains can be achieved when the intensity ratio β_1 and β_2 are certain values given in the caption of Fig. 4. In Fig. 4, as β_1 and β_2 decrease to zero, which is equivalent to seeding vacuum fields to the conjugate ports in the phase-insensitive cascaded scheme, the squeezing levels of intensity difference for different intensity gains will decrease nearly about 3 dB. That is to say, nearly 3 dB enhancement on the squeezing levels of intensity difference among the three output beams can be achieved in this phase-sensitive cascaded scheme compared to the phase-insensitive cascaded scheme with the same gain value [32]. Compared with the degree of intensity difference squeezing of the twin beams obtained with a single cell in the PSA configuration (see Fig. 4 in [31]), the degree of intensity difference squeezing of the triple beams has also been enhanced clearly. As shown in Fig. 5, we can also plot the squeezing levels of intensity difference for different gains of 2, 3, 4, 5 in decibels as a function of φ_1 and φ_2 when β_1 and β_2 are certain values. When the phase φ_1 and φ_2 are close to $0,2\pi$, the maximal squeezing levels can be achieved. Otherwise, when they are close to π, the noise levels are even higher than SQL ($D_{(\hat{N}_{a_2}-\hat{N}_{b_2}-\hat{N}_{b_1})}=0$ dB), i.e., they are antisqueezed. It is clear that with higher gain, a higher squeezing level of intensity difference can be obtained as shown in both Figs. 4 and 5.

Then, we consider the more general situation when the intensity gain $G_1=G_2=G$ ($G\geqslant 1$). Here one can easily calculate the $D_{\hat{N}_{a_2}-\hat{N}_{b_2}-\hat{N}_{b_1}}$ from Eq. (7). The maximal squeezing can be easily calculated, which is thus given by

$$D_{\max 1}=10\log_{10}\left(\frac{1}{2G^2-1+2G\sqrt{G^2-1}}\right). \tag{17}$$

This value can be achieved when $\beta_1=\frac{G}{G+1}$, $\beta_2=\frac{1}{G+1}$, and $\varphi_1=\varphi_2=0,2\pi$.

We can also consider the squeezing level of the intensity sum. The degree of squeezing of the intensity sum among the three output light fields with respect to the SQL is given by

$$D_{\hat{N}_{a_2}+\hat{N}_{b_2}+\hat{N}_{b_1}}=10\log_{10}\left(\frac{\mathrm{Var}(\hat{N}_{a_2}+\hat{N}_{b_2}+\hat{N}_{b_1})}{\mathrm{Var}(\hat{N}_{a_2}+\hat{N}_{b_2}+\hat{N}_{b_1})_{\mathrm{SQL}}}\right). \tag{18}$$

Through the use of Eq. (7), we can easily calculate the term $\mathrm{Var}(\hat{N}_{a_2}+\hat{N}_{b_2}+\hat{N}_{b_1})$, and $\mathrm{Var}(\hat{N}_{a_2}+\hat{N}_{b_2}+\hat{N}_{b_1})_{\mathrm{SQL}}$ is just the sum of the mean value of the photon numbers of the three output light fields. The squeezing level of intensity sum $D_{(\hat{N}_{a_2}+\hat{N}_{b_2}+\hat{N}_{b_1})}$ also changes with φ_1, φ_2, β_1, and β_2. We find that the maximal squeezing levels of intensity sum are -11.439, -15.311, -17.923, and -19.913 dB which correspond to $G_1=G_2=2,3,4,5$ respectively. In the cases of $G_1=G_2=2,3,4,5$, the maximal squeezing degrees can be achieved when intensity ratio β_1 and β_2 are certain values and $\varphi_1=\varphi_2=\pi$. In Fig. 6, we plot the squeezing levels of intensity sum in decibels as a function of the intensity ratio β_1 and β_2 when $\varphi_1=\varphi_2=\pi$ for $G_1=G_2=2,3,4,5$. In the case of $\varphi_1=\varphi_2=\pi$, the maximal squeezing for different gains can be achieved when the intensity ratio β_1 and β_2 are certain values as given in the caption of Fig. 6. As shown in Fig. 7,

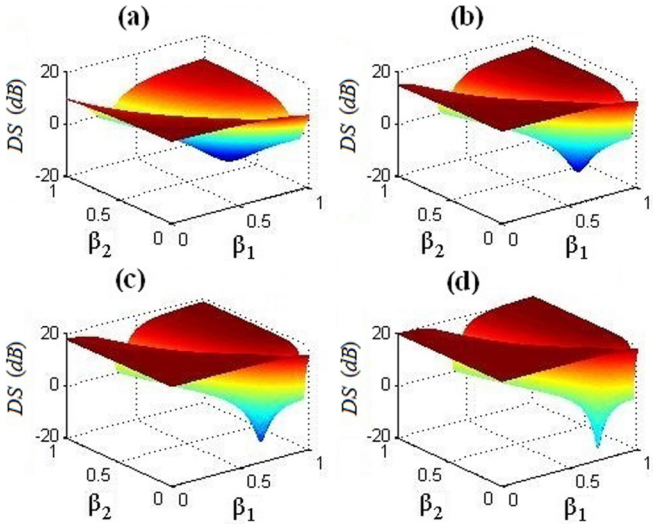

FIG. 6. The squeezing levels of intensity sum $D_{(\hat{N}_{a_2}+\hat{N}_{b_2}+\hat{N}_{b_1})}$ in decibels as a function of β_1 and β_2 when $\varphi_1 = \varphi_2 = \pi$. (a) $G_1 = G_2 = 2$: The squeezing level becomes maximal when $\beta_1 = 0.667$ and $\beta_2 = 0.333$. (b) $G_1 = G_2 = 3$: The squeezing level becomes maximal when $\beta_1 = 0.75$ and $\beta_2 = 0.25$. (c) $G_1 = G_2 = 4$: The squeezing level becomes maximal when $\beta_1 = 0.8$ and $\beta_2 = 0.2$. (d) $G_1 = G_2 = 5$: The squeezing level becomes maximal when $\beta_1 = 0.833$ and $\beta_2 = 0.167$.

we plot the squeezing levels of intensity sum in decibels for different intensity gains as a function of φ_1 and φ_2 when β_1 and β_2 are certain values. When the phase φ_1 and φ_2 are close to π, the maximal squeezing can be achieved. It can be seen from both Figs. 6 and 7 that the squeezing levels below the SQL can only be observed within very narrow ranges for both intensity ratios and phases. Also the squeezing levels of intensity sum

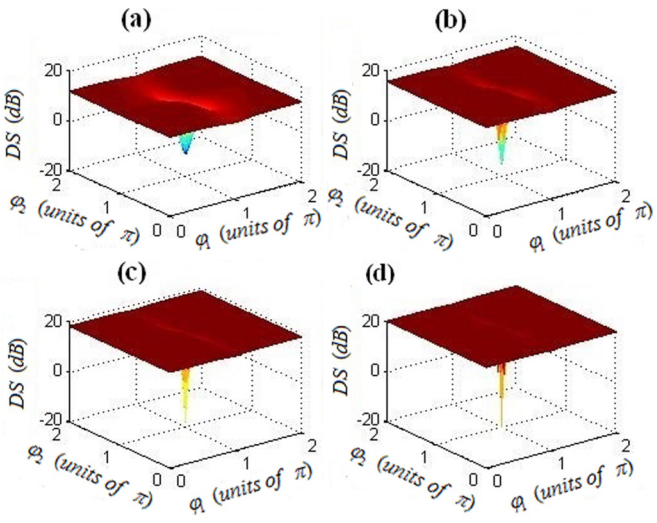

FIG. 7. (a) $G_1 = G_2 = 2$: The squeezing level of intensity sum $D_{(\hat{N}_{a_2}+\hat{N}_{b_2}+\hat{N}_{b_1})}$ varies with the phase φ_1 and φ_2 when $\beta_1 = 0.667$ and $\beta_2 = 0.333$. (b) $G_1 = G_2 = 3$: The squeezing level varies with the phases when $\beta_1 = 0.75$ and $\beta_2 = 0.25$. (c) $G_1 = G_2 = 4$: The squeezing level varies with the phases when $\beta_1 = 0.8$ and $\beta_2 = 0.2$. (d) $G_1 = G_2 = 5$: The squeezing level varies with the phases when $\beta_1 = 0.833$ and $\beta_2 = 0.167$. All of the squeezing levels for different gains become maximal when $\varphi_1 = \varphi_2 = \pi$.

increase with the increase of intensity gains. However, the ranges of intensity sum squeezing for both intensity ratios and phases will become narrower with the increase of intensity gains. Similarly, we consider the more general situation of intensity sum squeezing when $G_1 = G_2 = G$. Here one can easily calculate $D_{(\hat{N}_{a_2}+\hat{N}_{b_2}+\hat{N}_{b_1})}$ from Eq. (7). We can also find the maximal squeezing which is given by

$$D_{\max 2} = 10\log_{10}\left(\frac{1}{2G^2 - 1 + 2G\sqrt{G^2-1}}\right). \quad (19)$$

This equation can be obtained under the conditions of $\beta_1 = \frac{G}{G+1}$, $\beta_2 = \frac{1}{G+1}$, and $\varphi_1 = \varphi_2 = \pi$.

From Eqs. (17) and (19) it is clear that the values of maximum intensity difference squeezing and maximum intensity sum squeezing are equal to each other. That is to say, we can always find the common maximal squeezing level between squeezing of intensity sum and intensity difference by changing phase φ_1 and φ_2 based on phase-sensitive cascaded FWM processes.

We now consider the two other combinatorial squeezing $D_{(\hat{N}_{a_2}-\hat{N}_{b_2}+\hat{N}_{b_1})}$ and $D_{(\hat{N}_{a_2}+\hat{N}_{b_2}-\hat{N}_{b_1})}$ among the three output light fields. The squeezing levels $D_{(\hat{N}_{a_2}-\hat{N}_{b_2}+\hat{N}_{b_1})}$ and $D_{(\hat{N}_{a_2}+\hat{N}_{b_2}-\hat{N}_{b_1})}$ are given by

$$D_{\hat{N}_{a_2}-\hat{N}_{b_2}+\hat{N}_{b_1}} = 10\log_{10}\left(\frac{\mathrm{Var}(\hat{N}_{a_2} - \hat{N}_{b_2} + \hat{N}_{b_1})}{\mathrm{Var}(\hat{N}_{a_2} - \hat{N}_{b_2} + \hat{N}_{b_1})_{\mathrm{SQL}}}\right) \quad (20)$$

and

$$D_{\hat{N}_{a_2}+\hat{N}_{b_2}-\hat{N}_{b_1}} = 10\log_{10}\left(\frac{\mathrm{Var}(\hat{N}_{a_2} + \hat{N}_{b_2} - \hat{N}_{b_1})}{\mathrm{Var}(\hat{N}_{a_2} + \hat{N}_{b_2} - \hat{N}_{b_1})_{\mathrm{SQL}}}\right). \quad (21)$$

Through use of Eq. (7), we can easily calculate these two squeezing levels. We also set $G_1 = G_2 = 2,3,4,5$ to study the influence of φ_1, φ_2, β_1, and β_2 on these two degrees of intensity squeezing. The values of maximum intensity squeezing -11.439, -15.311, -17.923, and -19.913 dB for gain 2, 3, 4, 5 respectively can be achieved when $\varphi_1 = \pi$, $\varphi_2 = 0,2\pi$, and β_1, β_2 are certain values in the case of intensity combination of $\hat{N}_{a_2} - \hat{N}_{b_2} + \hat{N}_{b_1}$. In Fig. 8, we set the phases of input beams φ_1 as π and φ_2 as $0/2\pi$ to study how the intensity ratio β_1 and β_2 affect the degrees of intensity squeezing. In the case of $\varphi_1 = \pi, \varphi_2 = 0,2\pi$, the maximal squeezing levels of $\hat{N}_{a_2} - \hat{N}_{b_2} + \hat{N}_{b_1}$ for gain 2, 3, 4, 5 can be achieved when the intensity ratio β_1 and β_2 are certain values as given in the caption of Fig. 8. We find that the noises of the intensity combination $\hat{N}_{a_2} - \hat{N}_{b_2} + \hat{N}_{b_1}$ for gain 2, 3, 4, 5 respectively could be well below the SQL within wide intensity ratio ranges. In Fig. 9, we set β_1 and β_2 as certain values to study the influence of the phases on the degrees of intensity squeezing. As $\varphi_1 = \pi$ and $\varphi_2 = 0/2\pi$, the maximal squeezing for different intensity gains can be achieved. In addition, another case is the intensity combination of $\hat{N}_{a_2} + \hat{N}_{b_2} - \hat{N}_{b_1}$. The maximal squeezing -11.439, -15.311, -17.923, and -19.913 dB for gain 2, 3, 4, 5 respectively can be achieved when β_1, β_2 are certain values and $\varphi_1 = \varphi_2 = \pi$. In Fig. 10, the squeezing levels vary with the intensity ratios for $\varphi_1 = \varphi_2 = \pi$. In the case of $\varphi_1 = \varphi_2 = \pi$, the maximal squeezing levels of $\hat{N}_{a_2} + \hat{N}_{b_2} - \hat{N}_{b_1}$ for gain 2, 3, 4, 5 can be achieved

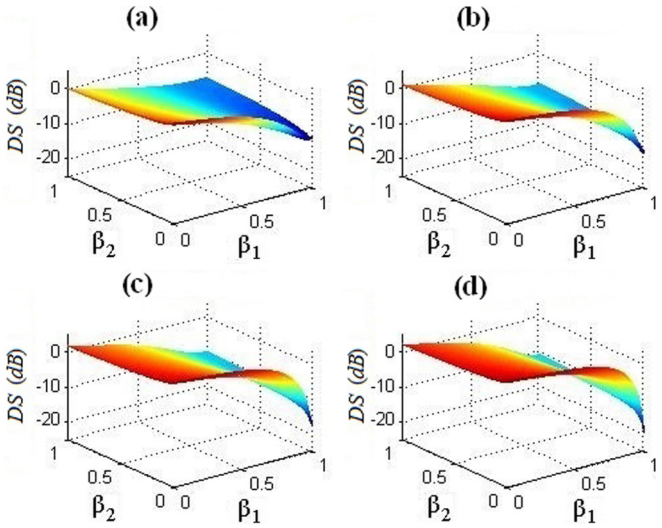

FIG. 8. The squeezing levels of $\hat{N}_{a_2} - \hat{N}_{b_2} + \hat{N}_{b_1}$ in decibels as a function of the intensity ratios when $\varphi_1 = \pi$ and $\varphi_2 = 0/2\pi$. (a) $G_1 = G_2 = 2$: The squeezing level becomes maximal when $\beta_1 = 0.988$ and $\beta_2 = 0.012$. (b) $G_1 = G_2 = 3$: The squeezing level becomes maximal when $\beta_1 = 0.997$ and $\beta_2 = 0.003$. (c) $G_1 = G_2 = 4$: The squeezing level becomes maximal when $\beta_1 = 0.998$ and $\beta_2 = 0.002$. (d) $G_1 = G_2 = 5$: The squeezing level becomes maximal when $\beta_1 = 0.999$ and $\beta_2 = 0.001$.

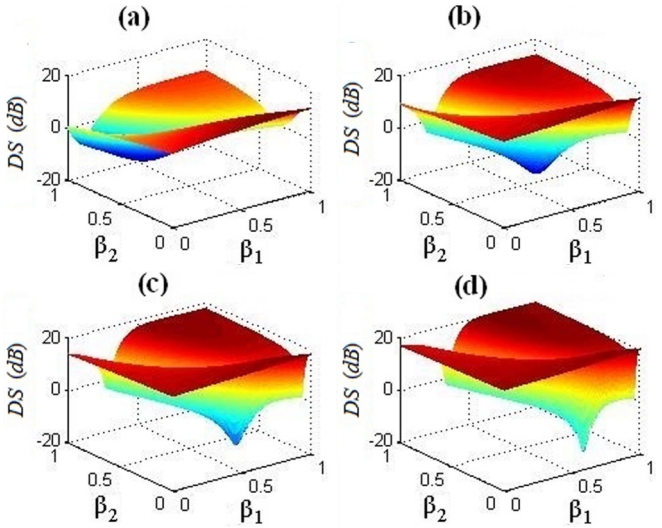

FIG. 10. The squeezing levels of $\hat{N}_{a_2} + \hat{N}_{b_2} - \hat{N}_{b_1}$ in decibels as a function of the ratios when $\varphi_1 = \varphi_2 = \pi$. (a) $G_1 = G_2 = 2$: The squeezing level becomes maximal when $\beta_1 = 0.301$ and $\beta_2 = 0.699$. (b) $G_1 = G_2 = 3$: The squeezing level becomes maximal when $\beta_1 = 0.564$ and $\beta_2 = 0.436$. (c) $G_1 = G_2 = 4$: The squeezing level becomes maximal when $\beta_1 = 0.69$ and $\beta_2 = 0.31$. (d) $G_1 = G_2 = 5$: The squeezing level becomes maximal when $\beta_1 = 0.761$ and $\beta_2 = 0.239$.

when the intensity ratio β_1 and β_2 are certain values given in the caption of Fig. 10. In Fig. 11, we set β_1 and β_2 are certain values to study the influence of the phases on the degrees of intensity squeezing. Obviously, the maximal squeezing levels can be achieved when $\varphi_1 = \varphi_2 = \pi$. As shown in both Figs. 10 and 11, the squeezing levels below the SQL can only be observed within very narrow ranges for both intensity ratios and phases. The squeezing levels of intensity combination of $\hat{N}_{a_2} + \hat{N}_{b_2} - \hat{N}_{b_1}$ will increase and the ranges of intensity squeezing for both intensity ratios and

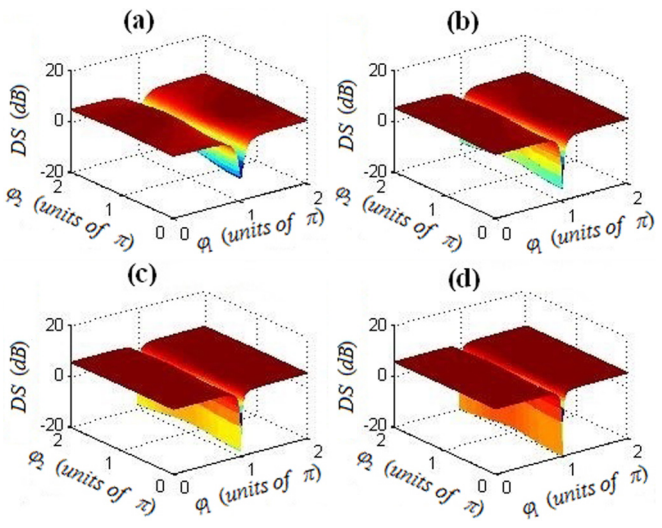

FIG. 9. (a) $G_1 = G_2 = 2$: The squeezing level of $\hat{N}_{a_2} - \hat{N}_{b_2} + \hat{N}_{b_1}$ varies with the phases when $\beta_1 = 0.988$ and $\beta_2 = 0.012$. (b) $G_1 = G_2 = 3$: The squeezing level varies with the phases when $\beta_1 = 0.997$ and $\beta_2 = 0.003$. (c) $G_1 = G_2 = 4$: The squeezing level varies with the phases when $\beta_1 = 0.998$ and $\beta_2 = 0.002$. (d) $G_1 = G_2 = 5$: The squeezing level varies with the phases when $\beta_1 = 0.999$ and $\beta_2 = 0.001$. All of the squeezing levels for different gains become maximal when $\varphi_1 = \pi$ and $\varphi_2 = 0/2\pi$.

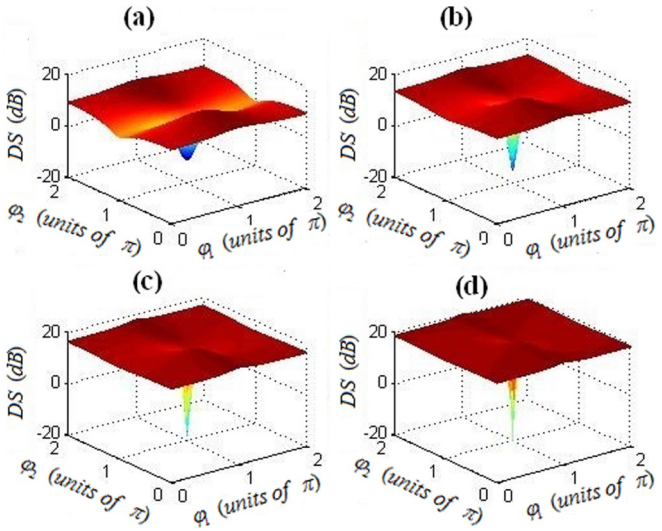

FIG. 11. (a) G_1=G_2=2: The squeezing level of $\hat{N}_{a_2}$+$\hat{N}_{b_2}$−$\hat{N}_{b_1}$ in decibels as a function of the phases when $\beta_1 = 0.301$ and $\beta_2 = 0.699$. (b) $G_1 = G_2 = 3$: The squeezing level varies with the phases when $\beta_1 = 0.564$ and $\beta_2 = 0.436$. (c) $G_1 = G_2 = 4$: The squeezing level of varies with the phases when $\beta_1 = 0.69$ and $\beta_2 = 0.31$. (d) $G_1 = G_2 = 5$: The squeezing level varies with the phases when $\beta_1 = 0.761$ and $\beta_2 = 0.239$. All of the squeezing levels for different gains become maximal when $\varphi_1 = \varphi_2 = \pi$.

phases will become narrower with the increase of intensity gains.

Then, we consider the general situation when the intensity gain $G_1 = G_2 = G$. The maximal squeezing of $\hat{N}_{a_2} - \hat{N}_{b_2} + \hat{N}_{b_1}$ and $\hat{N}_{a_2} + \hat{N}_{b_2} - \hat{N}_{b_1}$ can be calculated, which through use of Eqs. (7), (20), and (21) becomes

$$D_{\max 3} = 10\log_{10}\left(\frac{1}{2G^2 - 1 + 2G\sqrt{G^2-1}}\right). \quad (22)$$

The maximal squeezing values of these two combinations are equal to each other. In the case of $\hat{N}_{a_2} - \hat{N}_{b_2} + \hat{N}_{b_1}$, the maximal squeezing can be achieved when

$$\beta_1 = \frac{G(-3-4G+8G^2) + 4G(2G-1)\sqrt{G^2-1}}{1+G(-3-4G+8G^2) + 4G(2G-1)\sqrt{G^2-1}}, \quad (23)$$

$$\beta_2 = \frac{1}{1+G(-3-4G+8G^2) + 4G(2G-1)\sqrt{G^2-1}}, \quad (24)$$

$\varphi_1 = \pi$, and $\varphi_2 = 0, 2\pi$. Then in the case of $\hat{N}_{a_2} + \hat{N}_{b_2} - \hat{N}_{b_1}$, the maximal squeezing can be achieved when

$$\beta_1 = \frac{G(-3-4G+8G^2) - 4G(2G-1)\sqrt{G^2-1}}{1+G(-3-4G+8G^2) - 4G(2G-1)\sqrt{G^2-1}}, \quad (25)$$

$$\beta_2 = \frac{1}{1+G(-3-4G+8G^2) - 4G(2G-1)\sqrt{G^2-1}}, \quad (26)$$

and $\varphi_1 = \varphi_2 = \pi$. It is clear that the values of various combinatorial maximum squeezing are equal when the intensity gain of the two FWM processes is fixed. That is to say, by changing the phases and intensities of the input beams, we can always get the same maximum squeezing level for any combination of the intensity of the output fields.

It is interesting to examine how this maximum squeezing level varies with the gain parameter $G_1 = G_2 = G$ ($G \geqslant 1$). These results are summarized in Fig. 12. For $G = 1$ (no gain), the maximal squeezing level is equal to zero, showing that there is no squeezing. When the gain is greater than 1, the degree of the maximum squeezing can be improved. For the special cases when the intensity gain $G = 2,3,4,5$, the maximal squeezing degrees are -11.439, -15.311, -17.923, and -19.913 dB respectively. This is consistent with the results of our earlier calculations in this paper.

We also consider losses that occur in the two Rb cells (atomic absorption) and after mixing (imperfect optical transmission and detection efficiency). The losses that occur after mixing are modeled by a beamsplitter with an empty port [42] whose output state is a combination of the input and vacuum modes. For simplicity, we also consider the atomic absorption in two Rb cells as a beamsplitter with an empty port, contributing vacuum fluctuations to the transmitted beams. Denoting the vacuum modes introduced by losses on the probe and conjugate by the annihilation operators $\hat{v}_i$ ($i = 1-8$) respectively [43], the standard beamsplitter

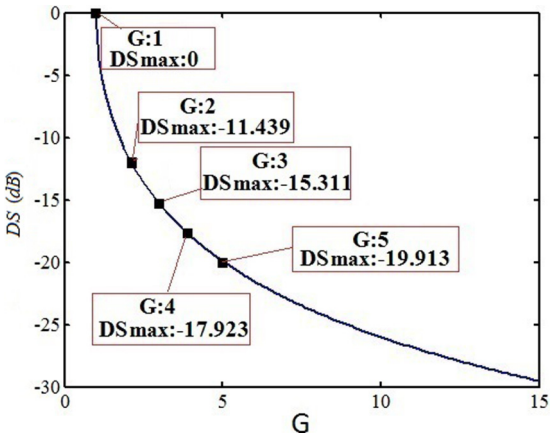

FIG. 12. Value of maximum squeezing degree as predicted by Eqs. (17), (19), and (22) plotted against the intensity gain G when only $G \geqslant 1$ is considered.

input-output relations give

$$\begin{aligned}
\hat{a}_1(t) &\to \sqrt{\eta_1}(\sqrt{L_1}\hat{a}_1 + \sqrt{1-L_1}\hat{v}_1) + \sqrt{1-\eta_1}\hat{v}_2,\\
\hat{b}_1(t) &\to \sqrt{\eta_2}(\sqrt{L_2}\hat{b}_1 + \sqrt{1-L_2}\hat{v}_3) + \sqrt{1-\eta_2}\hat{v}_4,\\
\hat{a}_2(t) &\to \sqrt{\eta_3}(\sqrt{L_3}\hat{a}_2 + \sqrt{1-L_3}\hat{v}_5) + \sqrt{1-\eta_3}\hat{v}_6,\\
\hat{b}_2(t) &\to \sqrt{\eta_4}(\sqrt{L_4}\hat{b}_2 + \sqrt{1-L_4}\hat{v}_7) + \sqrt{1-\eta_4}\hat{v}_8. \quad (27)
\end{aligned}$$

Here η_1, η_2, η_3, and η_4 are the transmission ratios of the light beam intensities due to the imperfect optical transmission and detection efficiency. L_1, L_2, L_3, and L_4 stand for the transmission ratios in the two Rb cells for probe and conjugate fields. For simplicity, we consider all the transmission ratios $\eta_1, \eta_2, \eta_3, \eta_4$ after mixing as η and all the transmission ratios L_1, L_2, L_3, L_4 in two Rb cells as L. Then we can easily calculate the maximal squeezing levels of different intensity combinations followed by optical losses. The values of maximum squeezing degrees of different intensity combinations corresponding to our phase-sensitive cascaded scheme followed by optical losses are similar. In Fig. 13, we plot the maximum squeezing level in decibels as a function of the gain parameter G followed by optical losses in the system. The blue curve shows the maximal squeezing level when the transmission ratio η and L are equal to 1, meaning

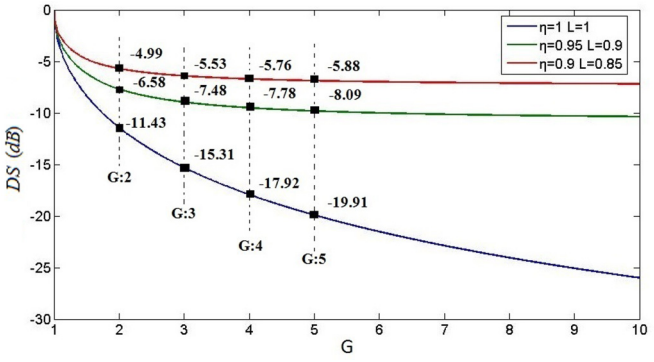

FIG. 13. Values of maximum squeezing degree followed by optical losses plotted against the intensity gain G.

that there are no losses. As shown in Fig. 13, the values of maximum squeezing degree decrease when $\eta = 0.95$, $L = 0.9$ (green curve) or $\eta = 0.9$, $L = 0.85$ (red curve). When the transmission ratio η is equal to 0.95 and L is equal to 0.9, the maximal squeezing is -6.58, -7.48, -7.78, and -8.09 dB for intensity gain $G = 2,3,4,5$ respectively. When η decreases to 0.9 and L decreases to 0.85, the maximal squeezing decreases to -4.99, -5.53, -5.76, and -5.88 dB for intensity gain $G = 2,3,4,5$ respectively.

V. GENUINE TRIPARTITE ENTANGLEMENT AND STEERING

In the above sections, we have discussed the intensity quantum correlations between the three output fields from the cascaded FWM processes. Multipartite entanglement is the fundamental ingredient for the future quantum networks [3]. Therefore, it is worth studying the possibility of generating tripartite entanglement from our cascaded FWM processes. Here we will use the single-condition and two-condition criteria [33] to characterize the tripartite entanglement of our system in the continuous variable regime. The amplitude and phase quadrature operators of the fields are defined by

$$\hat{X}_i = \frac{1}{\sqrt{2}}(\hat{O}_i^\dagger + \hat{O}_i), \quad \hat{Y}_i = \frac{i}{\sqrt{2}}(\hat{O}_i^\dagger - \hat{O}_i). \tag{28}$$

First, let us discuss the condition for the tripartite entanglement in our phase-sensitive cascaded FWM processes by using the single-condition criterion [33]. Using our quadrature definitions above, the single-condition criterion gives a set of formulas

$$\begin{aligned}
V_{123} &= V\left(\hat{X}_1 - \frac{1}{\sqrt{2}}(\hat{X}_2 + \hat{X}_3)\right) + V\left(\hat{Y}_1 + \frac{1}{\sqrt{2}}(\hat{Y}_2 + \hat{Y}_3)\right),\\
V_{213} &= V\left(\hat{X}_2 - \frac{1}{\sqrt{2}}(\hat{X}_1 + \hat{X}_3)\right) + V\left(\hat{Y}_2 + \frac{1}{\sqrt{2}}(\hat{Y}_1 + \hat{Y}_3)\right),\\
V_{312} &= V\left(\hat{X}_3 - \frac{1}{\sqrt{2}}(\hat{X}_1 + \hat{X}_2)\right) + V\left(\hat{Y}_3 + \frac{1}{\sqrt{2}}(\hat{Y}_1 + \hat{Y}_2)\right).
\end{aligned} \tag{29}$$

If one of the formulas in Eq. (29) is less than 1, we could claim that there exists genuine tripartite entanglement in our system. The dependence of V_{123} on the gains G_1, G_2 and phase θ_1' (equal to $\theta_1 + \theta_x$), θ_2 can be written as

$$\begin{aligned}
V_{123} = {} & 3G_1G_2 - 1 + 2\sqrt{G_1(G_1-1)(G_2-1)}\cos(\theta_1' - \theta_2)\\
& - 2\sqrt{2}\sqrt{G_1G_2(G_1-1)}\cos\theta_1'\\
& - 2\sqrt{2}G_1\sqrt{G_2(G_2-1)}\cos\theta_2.
\end{aligned} \tag{30}$$

Let us set $G_1 = G_2 = 2,3,4,5$ respectively to study the influence of θ_1' and θ_2 on the tripartite entanglement in our phase-sensitive cascaded system. The contour plot of V_{123} is shown in Fig. 14, the values of V_{123} for intensity gain 2, 3, 4, 5 are less than 1 (shown as white region) when the θ_1' and θ_2 are close to 0 and 2π. The ranges of tripartite entanglement for phase θ_1' and θ_2 will become narrower with the increase of intensity gain G. Then we set $\theta_1' = \theta_2 = 0/2\pi$ to study the influence of G_1 and G_2 on the tripartite entanglement in our phase-sensitive cascaded system. The V_{123} can be written as

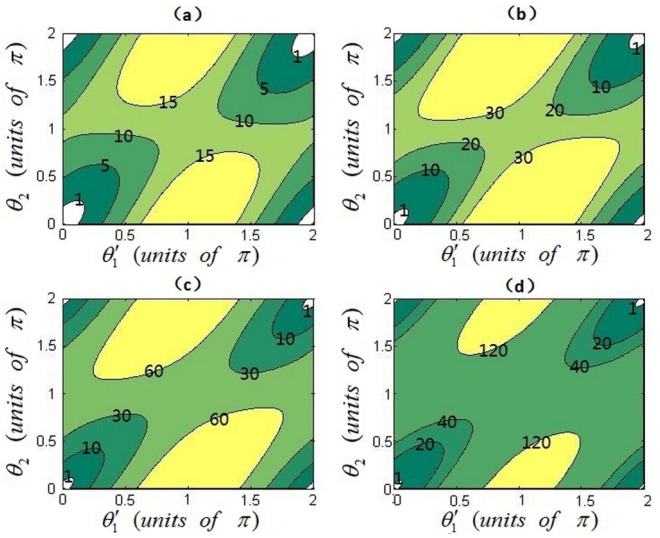

FIG. 14. Contour plot for V_{123} when the intensity gains $G_1 = G_2 = 2$ (a), $G_1 = G_2 = 3$ (b), $G_1 = G_2 = 4$ (c), and $G_1 = G_2 = 5$ (d) respectively. The white regions ($V_{123} < 1$) are the regions of the existence of tripartite entanglement.

$$\begin{aligned}
V_{123} = {} & 3G_1G_2 - 1 + 2\sqrt{G_1(G_1-1)(G_2-1)}\\
& - 2\sqrt{2}\sqrt{G_1G_2(G_1-1)} - 2\sqrt{2}G_1\sqrt{G_2(G_2-1)}.
\end{aligned} \tag{31}$$

Its contour plot is shown as Fig. 15. The values of most of the region are less than 1 as shown in Fig. 15, which correspond to the existence of entanglement for the three output light beams in our phase-sensitive cascaded system when $\theta_1' = \theta_2 = 0/2\pi$. It is already sufficient for proving the existence of tripartite entanglement for the three output light beams as shown in both Figs. 14 and 15. In addition, when the conjugate ports $\hat{b}_0$

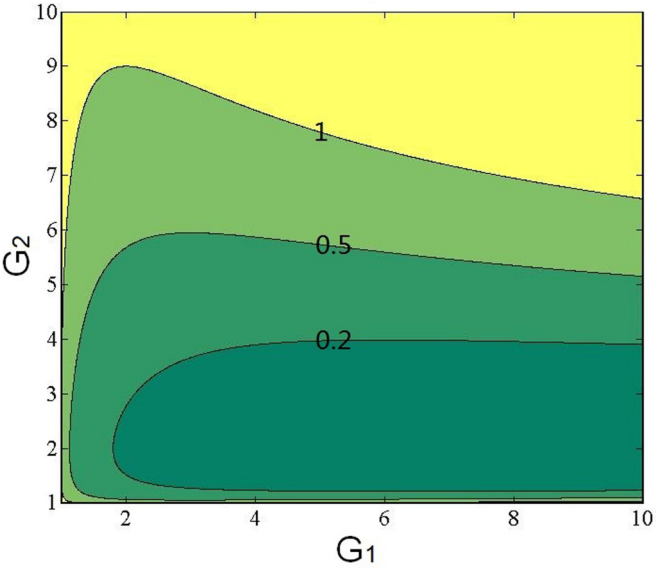

FIG. 15. Contour plot for V_{123} as a function of G_1 and G_2 when $\theta_1' = \theta_2 = 0/2\pi$.

and $\hat{b}_0'$ are seeded with vacuums, the phase-sensitive cascaded scheme will be translated into the phase-insensitive cascaded scheme. It is interesting to find that the dependence of V_{123} on the gains G_1 and G_2 in the phase-insensitive cascaded scheme through the use of Eq. (29) is consistent with Eq. (31). That is to say, there also exists multipartite entanglement for the three output light beams in the phase-insensitive cascaded system. Therefore, its contour plot is also shown as Fig. 15.

Then we discuss the condition for the tripartite entanglement in our phase-sensitive cascaded FWM processes by using the two-condition criterion [33]. Using our quadrature definitions in Eq. (28), the two-condition criterion can give a set of formulas

$$V_{12} = V(\hat{X}_1 - \hat{X}_2) + V(\hat{Y}_1 + \hat{Y}_2 + F_3\hat{Y}_3),$$
$$V_{13} = V(\hat{X}_1 - \hat{X}_3) + V(\hat{Y}_1 + F_2\hat{Y}_2 + \hat{Y}_3). \tag{32}$$

Here F_i $(i = 2,3)$ are arbitrary real numbers. It is sufficient to demonstrate genuine tripartite entanglement in our phase-sensitive cascaded system when both of the above formulas in Eq. (32) are less than 2. We can optimize the two-condition criterion using the freedom allowed in the choice of the F_i. Through the direct differentiation for Eq. (32) with respect to the F_i, we get the expressions of optimal F_i which are given by

$$F_2 = \frac{\cos\theta_2 G_1\sqrt{G_2(G_2-1)} - \cos(\theta_1' - \theta_2)\sqrt{G_1(G_1-1)(G_2-1)}}{G_1G_2 - G_1 + 0.5},$$
$$F_3 = \frac{\cos\theta_1' G_1\sqrt{G_2(G_1-1)} - \cos(\theta_1' - \theta_2)\sqrt{G_1(G_1-1)(G_2-1)}}{G_1 - 0.5}. \tag{33}$$

We set $G_1 = G_2 = 2,3,4,5$ to study the dependence of V_{12} and V_{13} on θ_1' and θ_2 in our phase-sensitive cascaded system. In Fig. 16, we study the influence of θ_1' and θ_2 on the V_{12} for $G_1 = G_2 = 2,3,4,5$ respectively. The white regions are the regions of $V_{12} < 2$. In Fig. 17, we study the influence of θ_1' and θ_2 on the V_{13} for $G_1 = G_2 = 2,3,4,5$ respectively. We can see that there exists the region of $V_{13} < 2$ only for $G_1 = G_2 = 2$. So there will be overlapped regions of $V_{12} < 2$ and $V_{13} < 2$ only when $G_1 = G_2 = 2$ as shown in both Figs. 16(a) and 17(a), meaning that the genuine tripartite entanglement is present only for $G_1 = G_2 = 2$ by using the two-condition criterion. The overlapped regions of $V_{12} < 2$ and $V_{13} < 2$ exist when θ_1' and θ_2 are close to $0/2\pi$. Therefore we set $\theta_1' = \theta_2 = 0/2\pi$ to study the dependence of V_{12} and V_{13} on G_1 and G_2 in our phase-sensitive cascaded scheme. As shown in Figs. 18(a) and 18(b), the V_{12} and V_{13} are plotted as a function of the G_1 and G_2 when $\theta_1' = \theta_2 = 0/2\pi$. In Fig. 18(c), we give the overlapped regions of $V_{12} < 2$ and $V_{13} < 2$ when $\theta_1' = \theta_2 = 0/2\pi$. The overlapped region (white region) shows that the genuine tripartite entanglement is present in our phase-sensitive cascaded system. As mentioned above, the phase-sensitive cascaded scheme will be translated into the phase-insensitive cascaded scheme when the conjugate ports $\hat{b}_0$ and $\hat{b}_0'$ are seeded with vacuums. Similarly, we can find that the dependence of V_{12} and V_{13} on the gains G_1 and G_2 in the phase-insensitive cascaded system through use of Eq. (32) is consistent with the cases of the phase-sensitive cascaded system when $\theta_1' = \theta_2 = 0/2\pi$.

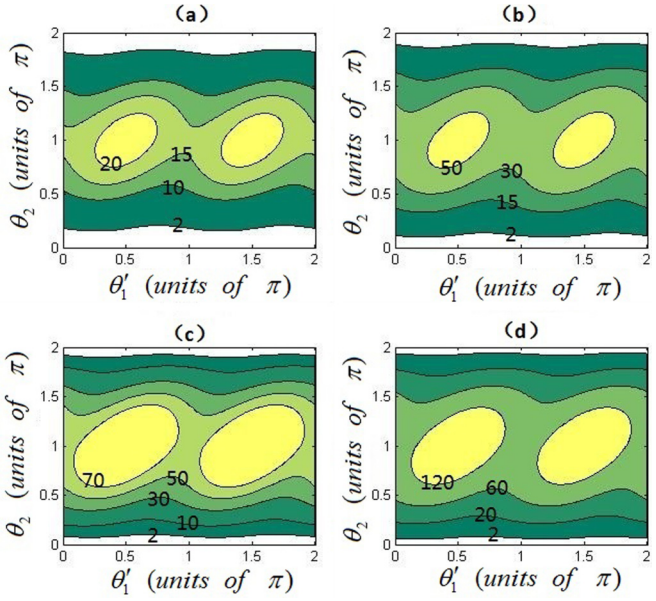

FIG. 16. Contour plot for V_{12} in Eq. (32) when the intensity gains $G_1 = G_2 = 2$ (a), $G_1 = G_2 = 3$ (b), $G_1 = G_2 = 4$ (c), and $G_1 = G_2 = 5$ (d) respectively. The white regions are the regions of $V_{12} < 2$.

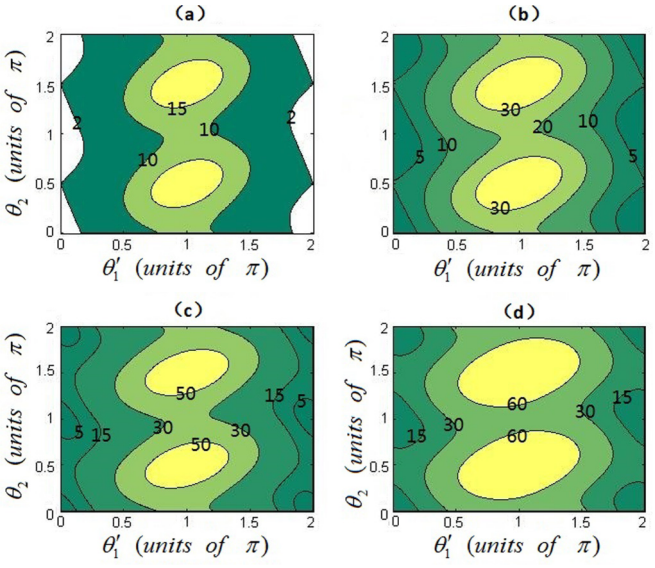

FIG. 17. Contour plot for V_{13} in Eq. (32) when the intensity gains $G_1 = G_2 = 2$ (a), $G_1 = G_2 = 3$ (b), $G_1 = G_2 = 4$ (c), and $G_1 = G_2 = 5$ (d) respectively.

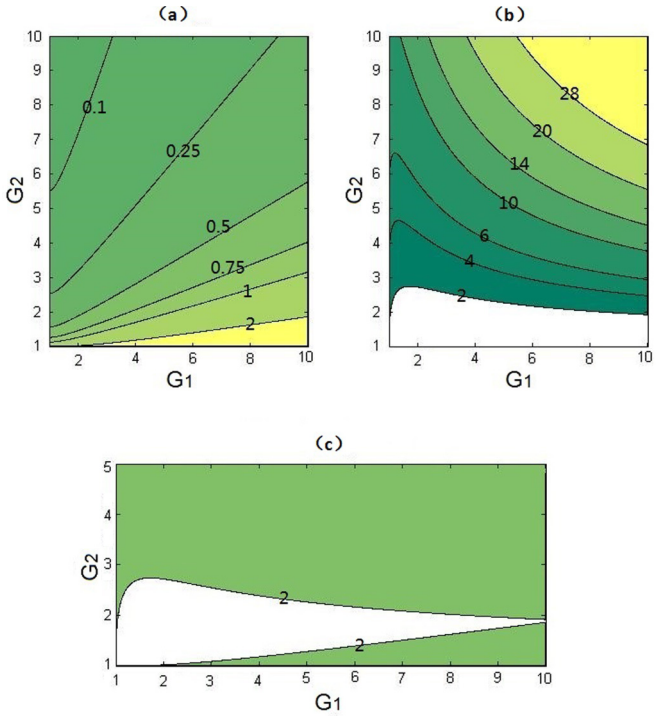

FIG. 18. The values of V_{12} (a) and V_{13} (b) in Eq. (32) vary with G_1 and G_2 when $\theta_1' = \theta_2 = 0/2\pi$. (c) The white region is the overlapped region of $V_{12} < 2$ and $V_{13} < 2$.

That is to say, there also exists genuine tripartite entanglement in the phase-insensitive cascaded system.

Further, due to the importance of multipartite steering for understanding entanglement distribution and constructing quantum networks [4], we investigate the possibilities of the existence of genuine multipartite steering in our phase-sensitive cascaded FWM scheme. To confirm genuine tripartite steering, let us calculate the following formulas [34,35]:

$$\mathrm{St}_{123} = \Delta_{\mathrm{inf}}(\hat{X}_1)\Delta_{\mathrm{inf}}(\hat{Y}_1), \tag{34}$$

$$\mathrm{St}_{213} = \Delta_{\mathrm{inf}}(\hat{X}_2)\Delta_{\mathrm{inf}}(\hat{Y}_2), \tag{35}$$

$$\mathrm{St}_{312} = \Delta_{\mathrm{inf}}(\hat{X}_3)\Delta_{\mathrm{inf}}(\hat{Y}_3). \tag{36}$$

$\mathrm{St}_{123} < \frac{1}{2}$, $\mathrm{St}_{213} < \frac{1}{2}$, and $\mathrm{St}_{312} < \frac{1}{2}$ imply steerings $\hat{O}_2\hat{O}_3 \to \hat{O}_1$, $\hat{O}_1\hat{O}_3 \to \hat{O}_2$, and $\hat{O}_1\hat{O}_2 \to \hat{O}_3$ respectively. Here $\Delta_{\mathrm{inf}}(\hat{X}_i)$ and $\Delta_{\mathrm{inf}}(\hat{Y}_i)$ are the uncertainty in the prediction of amplitude quadrature $\hat{X}_i$ and phase quadrature $\hat{Y}_i$ of one light beam $[[\hat{X}_i, \hat{Y}_i] = i$, which can be deduced from Eq. (28)] based on measurements of the other two light beams [44–46], and they are given by

$$\Delta_{\mathrm{inf}}(\hat{X}_i) = \Delta(\hat{X}_i + g_{\mathrm{opt},\hat{X}_j}\hat{X}_j + g_{\mathrm{opt},\hat{X}_k}\hat{X}_k), \tag{37}$$

$$\Delta_{\mathrm{inf}}(\hat{Y}_i) = \Delta(\hat{Y}_i + g_{\mathrm{opt},\hat{Y}_j}\hat{Y}_j + g_{\mathrm{opt},\hat{Y}_k}\hat{Y}_k). \tag{38}$$

Here $g_{\mathrm{opt},\hat{X}_j}$ and $g_{\mathrm{opt},\hat{X}_k}$ ($g_{\mathrm{opt},\hat{Y}_j}$ and $g_{\mathrm{opt},\hat{Y}_k}$) are optimized real numbers. Then, according to Ref. [34], the existence of genuine tripartite steering can be confirmed if $\mathrm{St}_{123} + \mathrm{St}_{213} + \mathrm{St}_{312} < \frac{1}{2}$. As shown in Figs. 19(a)–19(d), the St_{123}, St_{213}, St_{312} and $\mathrm{St}_{123} + \mathrm{St}_{213} + \mathrm{St}_{312}$ are plotted as a function of the G_1 and G_2 when $\theta_1' = \theta_2 = 0/2\pi$ in our phase-sensitive cascaded scheme. The values of all the region are less than $\frac{1}{2}$ as shown in Figs. 19(a)–19(c), which implies that the amplitude quadrature and phase quadrature of any one of the output beams is highly correlated with a combination of the other two output beams. The contour plot of $\mathrm{St}_{123} + \mathrm{St}_{213} + \mathrm{St}_{312}$ is shown in Fig. 19(d), the value of $\mathrm{St}_{123} + \mathrm{St}_{213} + \mathrm{St}_{312}$ is less than $\frac{1}{2}$ for most region of intensity gain G_1 and G_2, which corresponds to the existence of genuine tripartite steering in our phase-sensitive cascaded system when $\theta_1' = \theta_2 = 0/2\pi$. Similarly, we can find that the dependence of St_{123}, St_{213}, St_{312} and $\mathrm{St}_{123} + \mathrm{St}_{213} + \mathrm{St}_{312}$ on the gains G_1 and G_2 in the phase-insensitive cascaded scheme through use of Eqs. (34)–(36) is also consistent with the cases of the phase-sensitive cascaded system when $\theta_1' = \theta_2 = 0/2\pi$. That is to say, there also exists genuine tripartite steering in the phase-insensitive cascaded scheme.

VI. CONCLUSION

In this paper, we have studied an experimental scheme to generate three quantum correlated beams via a phase-sensitive cascaded FWM in hot Rb atomic vapor. We have shown some interesting results for quantum correlation existing in this system. Compared with the degree of intensity difference squeezing of the twin beams obtained with phase-sensitive single FWM process [31] or the three output beams obtained with phase-insensitive cascaded FWM processes [32], the degree of intensity difference squeezing of the three beams output from the current phase-sensitive cascaded FWM processes can be

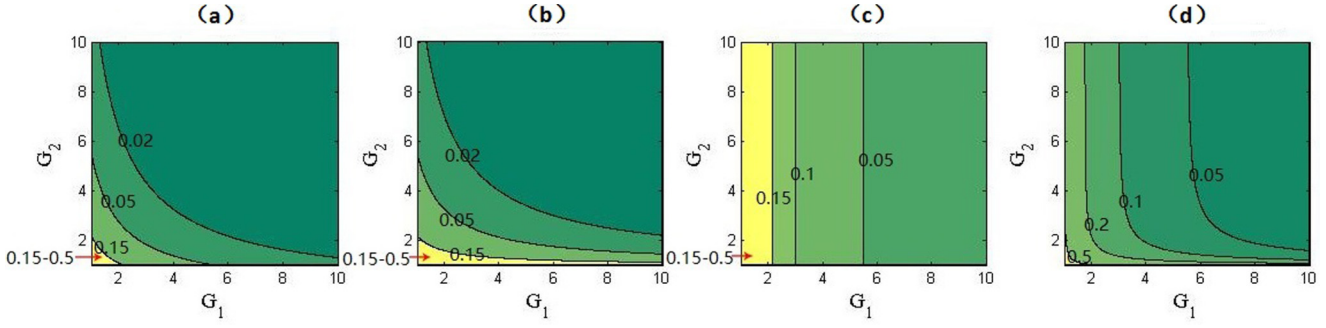

FIG. 19. The values of St_{123} (a), St_{213} (b), St_{312} (c) in Eqs. (34)–(36), and $St_{123} + St_{213} + St_{312}$ (d) vary with G_1 and G_2 when θ_1'=θ_2=$0/2\pi$.

largely enhanced. Beyond intensity difference squeezing, intensity sum squeezing and two other combinatorial squeezing among the three output light fields are predicted theoretically. The squeezing levels of different intensity combinations will increase with the increase of intensity gains. No matter what kind of combination, it is worth noting that the maximal squeezing levels would always refer to the same value when the intensity gain of the two FWM processes is fixed. The values of maximum squeezing degree will decrease followed by optical losses. Finally, we have also studied the genuine tripartite entanglement and steering in cascaded FWM processes. In order to experimentally realize our phase-sensitive cascaded scheme, we could exploit the coherent modulation phase locking technique for phase-sensitive FWM process that we have developed recently [47]. These findings may find applications in quantum metrology and quantum information processing due to its ability of quantum squeezing manipulation.

ACKNOWLEDGMENTS

We thank Q. He for useful discussions. This work was supported by the National Natural Science Foundation of China under Grants No. 91436211, No. 11374104, and No. 10974057, the SRFDP (20130076110011), the Program for Professor of Special Appointment (Eastern Scholar) at Shanghai Institutions of Higher Learning, the Program for New Century Excellent Talents in University (NCET-10-0383), the Shu Guang project supported by Shanghai Municipal Education Commission and Shanghai Education Development Foundation (11SG26), the Shanghai Pujiang Program under Grant No. 09PJ1404400, the Scientific Research Foundation of the Returned Overseas Chinese Scholars, State Education Ministry, National Basic Research Program of China (Grant No. 2016YFA030213), and the Program of State Key Laboratory of Advanced Optical Communication Systems and Networks (2016GZKF0JT003).

[1] A. Einstein, B. Podolsky, and N. Rosen, Phys. Rev. **47**, 777 (1935).
[2] D. M. Greenberger, M. A. Horne, and A. Zeilinger, Phys. Today **46**(8), 22 (1993).
[3] S. L. Braunstein and P. van Loock, Rev. Mod. Phys. **77**, 513 (2005).
[4] H. J. Kimble, Nature (London) **453**, 1023 (2008).
[5] P. van Loock and S. L. Braunstein, Phys. Rev. Lett. **84**, 3482 (2000).
[6] J. Jing, J. Zhang, Y. Yan, F. Zhao, C. Xie, and K. Peng, Phys. Rev. Lett. **90**, 167903 (2003).
[7] H. Yonezawa, T. Aoki, and A. Furusawa, Nature (London) **431**, 430 (2004).
[8] X. Su, A. Tan, X. Jia, J. Zhang, C. Xie, and K. Peng, Phys. Rev. Lett. **98**, 070502 (2007).
[9] S. Armstrong, J. F. Morizur, J. Janousek, B. Hage, N. Treps, P. K. Lam, and H. A. Bachor, Nat. Commun. **3**, 1026 (2012).
[10] M. Pysher, Y. Miwa, R. Shahrokhshahi, R. Bloomer, and O. Pfister, Phys. Rev. Lett. **107**, 030505 (2011).
[11] O. Pinel, P. Jian, R. M. de Araujo, J. Feng, B. Chalopin, C. Fabre, and N. Treps, Phys. Rev. Lett. **108**, 083601 (2012).
[12] S. Yokoyama, R. Ukai, S. C. Armstrong, C. Sornphiphatphong, T. Kaji, S. Suzuki, J. i. Yoshikawa, H. Yonezawa, N. C. Menicucci, and A. Furusawa, Nat. Photon. **7**, 982 (2013).
[13] M. Chen, N. C. Menicucci, and O. Pfister, Phys. Rev. Lett. **112**, 120505 (2014).
[14] J. Roslund, R. M. de Araujo, S. F. Jiang, C. Fabre, and N. Treps, Nat. Photon. **8**, 109 (2014).
[15] C. F. McCormick, V. Boyer, E. Arimondo, and P. D. Lett, Opt. Lett. **32**, 178 (2007).
[16] V. Boyer, A. M. Marino, R. C. Pooser, and P. D. Lett, Science **321**, 544 (2008).
[17] A. M. Marino, R. C. Pooser, V. Boyer, and P. D. Lett, Nature **457**, 859 (2009).
[18] J. Jing, C. Liu, Z. Zhou, Z. Y. Ou, and W. Zhang, Appl. Phys. Lett. **99**, 011110 (2011).
[19] J. Kong, J. Jing, H. Wang, C. Liu, and W. Zhang, Appl. Phys. Lett. **102**, 011130 (2013).
[20] F. Hudelist, J. Kong, C. Liu, J. Jing, Z. Y. Ou, and W. Zhang, Nat. Commun. **5**, 3049 (2014).
[21] A. MacRae, T. Brannan, R. Achal, and A. I. Lvovsky, Phys. Rev. Lett. **109**, 033601 (2012).
[22] R. C. Pooser and B. Lawrie, Optica **2**, 393 (2015).
[23] C. S. Embrey, M. T. Turnbull, P. G. Petrov, and V. Boyer, Phys. Rev. X **5**, 031004 (2015).
[24] L. M. Duan, M. D. Lukin, J. I. Cirac, and P. Zoller, Nature (London) **414**, 413 (2001).
[25] D. M. Greenberger, M. A. Horne, and A. Zeilinger, in *Bell's Theorem, Quantum Theory and Conceptions of the Universe*, edited by M. Kafatos (Kluwer, Dordrecht, 1989), pp. 69–72.
[26] C. Weedbrook, S. Pirandola, R. G. Patron, N. J. Cerf, T. C. Ralph, J. H. Shapiro, and S. Lloyd, Rev. Mod. Phys. **84**, 621 (2012).
[27] M. D. Lukin, Rev. Mod. Phys. **75**, 457 (2003).
[28] J. W. Pan, Z. B. Chen, C. Y. Lu, H. Weinfurter, A. Zeilinger, and M. Zukowski, Rev. Mod. Phys. **84**, 777 (2012).
[29] R. Pooser and J. Jing, Phys. Rev. A **90**, 043841 (2014).
[30] Y. Cai, J. Feng, H. Wang, G. Ferrini, X. Xu, J. Jing, and N. Treps, Phys. Rev. A **91**, 013843 (2015).
[31] Y. Fang and J. Jing, New J. Phys. **17**, 023027 (2015).
[32] Z. Qin, L. Cao, H. Wang, A. M. Marino, W. Zhang, and J. Jing, Phys. Rev. Lett. **113**, 023602 (2014).
[33] P. van Loock and A. Furusawa, Phys. Rev. A **67**, 052315 (2003).
[34] Q. Y. He and M. D. Reid, Phys. Rev. Lett. **111**, 250403 (2013).
[35] S. Armstrong, M. Wang, R. Y. Teh, Q. Gong, Q. He, J. Janousek, H. A. Bachor, M. D. Reid, and P. K. Lam, Nat. Phys. **11**, 167 (2015).
[36] H. Chen and J. Zhang, Phys. Rev. A **79**, 063826 (2009).
[37] J. A. Levenson, I. Abram, T. Rivera, and P. Grangier, J. Opt. Soc. Am. B **10**, 2233 (1993).
[38] R. W. Boyd, Z. Shi, and P. W. Milonni, J. Opt. **12**, 104007 (2010).
[39] C. M. Caves, Phys. Rev. D **26**, 1817 (1982).

[40] S. K. Choi, M. Vasilyev, and P. Kumar, Phys. Rev. Lett. **84**, 1361 (1999).
[41] C. J. McKinstrie, M. Yu, M. G. Raymer, and S. Radic, Opt. Express **13**, 4986 (2005).
[42] H. A. Bachor and T. C. Ralph, *A Guide to Experiments in Quantum Optics* (Wiley-VCH, Weinheim, 2004).
[43] C. M. Caves, Phys. Rev. Lett. **45**, 75 (1980).
[44] H. M. Wiseman, S. J. Jones, and A. C. Doherty, Phys. Rev. Lett. **98**, 140402 (2007).
[45] E. G. Cavalcanti, S. J. Jones, H. M. Wiseman, and M. D. Reid, Phys. Rev. A **80**, 032112 (2009).
[46] M. D. Reid, Phys. Rev. A **40**, 913 (1989).
[47] H. Wang, A. M. Marino, and J. Jing, Appl. Phys. Lett. **107**, 121106 (2015).